Benomar, S.; Chieregato, A.; Masso, A.; Soriano Rodríguez, MD.; Vidal Moya, JA.; Blasco Lanzuela, T.; Issaadi, R.... (2020). Al2O3-Supported W-V-O bronzes catalysts for oxidative dehydrogenation of ethane. Catalysis Science & Technology. 10(23):8064-8076. https://doi.org/10.1039/d0cy01220c

Al_2O_3-Supported W-V-O bronzes catalysts for oxidative dehydrogenation of ethane

by

S. Benomar [a,b], A. Chieregato [a,c], A. Masso [a], M.D. Soriano [a], J. A. Vidal-Moya [a], T. Blasco [a], R. Issaadi [b], J. M. López Nieto [a,*]

[a)] Instituto de Tecnología Química, Universitat Politècnica de València-Consejo Superior de Investigaciones Científicas, Avenida de los Naranjos s/n, 46022 Valencia, España

[b)] Hydrogen Energy Applications Laboratory, Faculty of Technology, University of Blida 1, Algeria.

[c)] Current address: Total Research Center-Qatar (TRCQ), Qatar Science & Tecnology Park, Al Gharrafa, Doha, P.O. Box 9803, Qatar.

* To whom correspondence should be addressed: Email address: jmlopez@itq.upv.es

Abstract

Supported vanadium-containing hexagonal tungsten bronze were prepared for the first time, thanks to the combination of a new soft synthetic procedure and fine-tuned heat treatments. The characterization of het-treated samples indicates that both unsupported and Al_2O_3-supported materials present mainly vanadium containing crystals with hexagonal tungsten bronze (HTB) structure smaller in the supported materials. However, supported materials present smaller crystals compared to unsupported materials. Raman, Diffuse Reflectance UV-vis and EPR spectroscopies results suggest the presence of different V-species depending on the V-loading and catalyst composition. When used as catalysts for ethane oxidative dehydrogenation (ODH), selected supported vanadium-HTBs show selectivity to ethylene as high as 80% at ethane conversion around 18%. These values position these new materials as one of the most active and selective catalysts so far reported in the literature for ethane ODH over supported vanadium oxide catalysts.

Keywords: ODH of ethane, vanadium, hexagonal tungsten bronze, Al_2O_3 support

Introduction

Hexagonal tungsten bronzes (HTBs) have received considerable attention in several fields of materials science due to their open-tunnel structure and their mixed proton and electron conductivity. Moreover, they are intermediates in the production of tungsten lamp filaments [1-3] and more recently, have also found applications in catalysis.[4,5] In more detail, HTBs are non-stoichiometric oxides closely related to the Perovskites family that can be represented with the general formula A_nBO_x, where A is a cation (e.g. Li^+, Na^+, Cs^+, Ca^{2+}, NH_4^+, etc.), B is W and/or another transition-metal (e.g. V, Mo, Ti, Nb) [1-3,6,7] and x is close to, but less than 3. The structure of HTBs is made up of corner-sharing WO_6 octahedra which position themselves in the three-dimensional space to form three-sided and six-sided channels that give rise to tunnels running along the c direction.

Several procedures have been reported in the bibliography for the synthesis of HTBs. Solid-state syntheses (also referred to as *hard syntheses*) was the first to be used in the pioneering works of A. Magneli et al.,[8] whereas in the last three decades efforts have been made to develop *soft methodologies* carried out at milder temperatures and shorter time of synthesis.[9] Typically, this is achieved by hydrothermal methods, which have the advantage of allowing a better control on the preparation of complex multi-element bronzes.

Among the physicochemical parameters that govern the behavior of HTBs in the above-mentioned technological applications, the specific surface area plays an important role. For instance, higher surface area leads to better sensitivity to gas detection, enhanced electrochromic properties and higher catalytic activity. Accordingly, organic-template and hard-template routes have been explored to create internal porosity within the bulk oxide network of transition-metal oxides.[10] However, a main drawback of these methods is that

the removal of the template molecules from the pores often requires a final calcination step under air at relatively high temperature. Indeed, several inorganic phases of interest are metastable [11] and, as in the case of HTBs,[1-3] they evolve to more thermodynamically favored phases when calcined. Another way to increase the surface area of metal oxides is to deposit them on high surface area supports. Not only does this lead to a more efficient use of the active phase (usually much more expensive than the support), but it can also change the physicochemical properties of the metal oxides, as metal-support interactions might arise at the interface of the two solid phases.

Conventional methods to support metal oxides are impregnation of the support with the active phase -or its precursor(s)- followed by thermal treatments. Hydrothermal preparations of supported metal oxides are usually impossible because the support typically dissolves under these conditions. Moreover, if it is not the case, not all the metal oxide anchors on the surface of the support as it likely precipitates in solution leading to a mixture of supported and bulk metal oxide phases.

Alumina-supported hexagonal tungsten bronze with potassium as counter-ion (K_nWO_x) was reported in the '80s to be prepared by incipient impregnation with potassium tungstate followed by thermal treatment in H_2.[12] More recently, the formation of bulk (i.e., unsupported) hexagonal ammonium tungsten bronze, i.e. $(NH_4)_nWO_x$, by partial reduction of ammonium paratungstate (APT) has been studied in detail.[13] Meanwhile, our studies on the preparation of bulk substituted-HTBs by Raman spectroscopy revealed that vanadium can enter the oxide framework of *h*-WO_x through a solid-state reaction.[14,15]

With this in mind, we decided to investigate the preparation of unsupported and γ-alumina-supported hexagonal tungsten bronzes, partially substituted with vanadium, using a *soft* synthetic procedure combined with heat-treatments at moderate temperature (600°C) and

short time of synthesis (3 hours). To the best of our knowledge, this is a novel method of synthesis of bi-metallic HTBs and the first report on the synthesis and characterization of a substituted HTB as a supported oxide. As an example of the possible technological applications, these new materials were used as heterogeneous catalysts for the oxidative dehydrogenation (ODH) of ethane.

ODH of ethane is a reaction of great interest as it is considered as an alternative for industrial ethylene production.[16-20] This can be mainly carried out by using four type of catalytic systems: i) supported vanadium oxide;[20-24] ii) multicomponent Mo-V-Te(Sb)-Nb mixed oxides with an orthorhombic bronze structure (M1 phase);[25-27] iii) promoted and/or supported nickel oxide;[28-31] and iv) catalysts based on non-reducible metal oxides.[18] To date, ethane ODH is still not a commercial process due to a not-yet favorable economic competitiveness compared to well establish technologies like ethane steam cracking. Nonetheless, several approaches are being investigated to improve the catalytic performance in the ODH of short chain alkanes some of them using supported vanadium oxides catalysts.[17-20, 32-35] Thus, it has been proposed that the formation of two and three-dimensional VOx species on the surface of specific catalysts improves the selectivity to propene during the propane ODH by decreasing the consecutive reaction,[32-34] i.e. combustion of both propane and propene, providing new insights to narrow the gap with commercial technologies.[27,36]

Experimental

Synthesis of catalysts

Synthesis of unsupported and γ-Al_2O_3 supported V-substituted HTBs

Ammonium paratungstate (**APT**) hydrate ($(NH_4)_{10}H_2(W_2O_7)_6 \cdot xH_2O$, 99.99%), Vanadium (IV) oxide sulfate hydrate (**VS**) ($VOSO_4 \cdot xH_2O$, ≥99.99%), and oxalic acid (**OA**) (≥99.0%), were purchased from Sigma Aldrich. γ-Al_2O_3 was prepared by calcining at 700°C (ramp rate 1.5°C min^{-1}, hold for 10h) Aluminum Oxide Hydroxide ($Al_2O_3 \cdot xH_2O$) produced by Sasol (Catapal® B Alumina).

For supported materials, the amount of tungsten precursor to be used was chosen so as to reach the theoretical monolayer of W-atoms, generally defined as 11.6 μmol of metal per m^2 of support surface.[37] Overall, APT (5.3 g) was dispersed in milli-Q water (20.0g). Oxalic acid was used as reducing agent and it was added in a 2-to-1 molar ratio respect to the tungsten content. Vanadyl sulfate and γ-Al_2O_3 were added during the synthesis, according to the desired molar ratios. The solution containing the APT was let boil under reflux for 16h. Then, oxalic acid and vanadium (IV) oxide sulfate were added under stirring. After 20 min Al_2O_3 was added. At the end of the preparation, water was removed by rotavapor and the materials were dried at 110°C overnight. Initially, the catalysts were prepared using a V/W ratio of 0.2.

The obtained materials were heat-treated under N_2 at 600°C using a rate of 100ºC min^{-1} during 3 hours. The heat-treatment temperature was chosen according to previous results,[38] which show that the HTB-phase substituted with vanadium is stable up to 600°C under inert atmosphere.

The samples, named as **S-I**, **S-II** and **S-R2** were prepared from synthesis gel with a V/W atomic ratio of 0.2 varying the order o addition of oxalic acid, the vanadium salt and the reflux step. In addition, samples **S-R1** and **S-R3** were prepared as sample **S-R2**, but using synthesis gels with V/W atomic ratios of 0.1 and 0.3, respectively. The characteristics of catalysts are shown in Table 1. Unsupported samples, denoted as **N-I**, **N-II** and **N-R**, with a molar ratio V/W = 0.2, were prepared following procedures analogous to **S-**I, **S-II** and **S-R2** samples, respectively.

Synthesis of reference materials

Reference materials were synthesized and used both for characterization purposes and catalytic tests. Thus, a V-containing h-WO_3 bronze with HTB structure (named **WV-HT**) was prepared by hydrothermal synthesis.[14] Vanadium oxide supported on alumina (named **VOx/AL**), a benchmark catalyst used for the oxidative dehydrogenation of alkanes, was prepared by the impregnation method.[22] In addition, a γ-Al_2O_3-supported V-W-O mixed oxide catalysts (named **WV/AL**) was also prepared by impregnation.[39] A vanadium oxide supported on tungsten hexagonal bronze supported on alumina (named **V/W/AL**) was also prepared. Characterization of the mentioned reference materials is reported in Table S1 (Supporting Information).

Characterization of catalysts

The BET surface area of the samples, S_{BET}, was obtained in an automatic ASAP 2020 system from Micromeritics, following the BET method from N_2 adsorption isotherms at −196 ºC.

X-ray diffraction patterns (XRD) were collected using a Philips X'Pert diffractometer equipped with a graphite monochromator, operating at 40 kV and 45 mA and employing nickel-filtered Cu$K\alpha$ radiation (λ = 0.1542 nm).

Raman spectra were recorded in a Renishaw system 1000 "in via" attached to a microscope at ambient conditions (excited with an Ar^+ line at 514 nm and operated at a power of 20 mW).

Diffuse reflectance (DR) spectra in the UV–visible region were collected with a Shimazdu UV-2010 PC spectrophotometer equipped with a reflectance attachment.

The EPR spectra were recorded at room temperature in a Bruker EMX-12 spectrometer working at the X band, with a modulation frequency of 100 kHz and 1 G amplitude. DPPH (g= 2.0036) was used as standard to measure the g values. Quantitative analysis was carried out by double integration of the spectra, using $CuSO_4$ as an external standard.

Morphological and structural characterization of catalysts was carried out by Transmission Electron Microscopy (JEOL, model JEM-1010) and FSEM (ZEISS Ultra-55 field-emission scanning electron microscope). XEDS was performed with an Oxford LINK ISIS system connected to a JEOL 6300 electron microscope (with the SEMQUANT program to incorporate ZAF correction).

X-ray photoelectron spectroscopy (XPS) analyses were carried out in a Physical Electronics spectrometer (PHI 5700) with X-ray Mg Kα radiation (300W, 15 kV, 1253.6 eV) as the excitation source was used for high-resolution record. Measurements were conducted by a concentric hemispherical analyzer which operates in the constant pass energy mode at 29.35 eV, using a 720 μm diameter analysis area. All the signals were referenced to C1s signal at 284.5 eV.

Catalytic tests

The catalytic experiments for ethane oxidative dehydrogenation (EODH) were carried out in a fixed-bed tubular reactor, at atmospheric pressure, in the 350-450 ºC temperature range, using an ethane/oxygen/nitrogen molar ratio of 4/8/88 and a contact time, W/F, of 80 g_{cat} h $(mol_{C2})^{-1}$. Analysis of reactants and products was carried out by gas chromatography, using two chromatographic columns:[39,40] (i) Carbosieve-S (2.4 m x1.8 in) to separate N_2, O_2 and CO; and ii) Porapak QS (2.0 m x 1.8 in) to separate CO_2 and hydrocarbons.

Results and discussion

Catalyst characterization

Partial thermal reduction of ammonium paratungstate (APT) into the HTB phase was studied in details by I. M. Szilágyi et al.[13] It was demonstrated that the heating rate plays a pivotal role in the phase purity of the final oxide, since it controls the linking process of WO_6 octahedra of paratungstate ions. Following this study, we carried out a preliminary research on the formation of the unsupported vanadium-substituted HTB phase (*h*-WVO_x) as a bulk phase. To do so, an aqueous solution of APT was mixed with vanadyl sulfate (VS) and oxalic acid (OA) as the reducing agent,[14] followed by solvent evaporation (see experimental section). The dried solid was then heat-treated under nitrogen at 600 ºC using different heating rates, specifically 3, 10 and 100 °C/min. By XRD analyses (Fig. S1, supporting information) it is clear that the higher amount of the HTB phase (JCPDS: 33-1387) was obtained using a heating rate equal to 100°C min^{-1} (Fig. S1, patterns c-e). The heating time is also fundamental: holding the material at 600°C for 3 hours leads to the best phase purity (Fig. S1, pattern e); since at longer time, the hexagonal phase transforms into a

monoclinic phase (Fig. S1, pattern f). Therefore, the *h*-WVOx oxide were prepared under nitrogen flow, using a heating rate of 100 °C min^{-1} and holding the material at 600 °C for 3 hours.

The influence of the catalyst preparation procedure was studied by changing the order of incorporation of OA and/or VS as well as the reflux step. Figure 1 shows the XRD patterns of heat-treated catalysts, i.e. unsupported (Fig. 1A) and Al_2O_3-supported (Fig. 1B) materials.

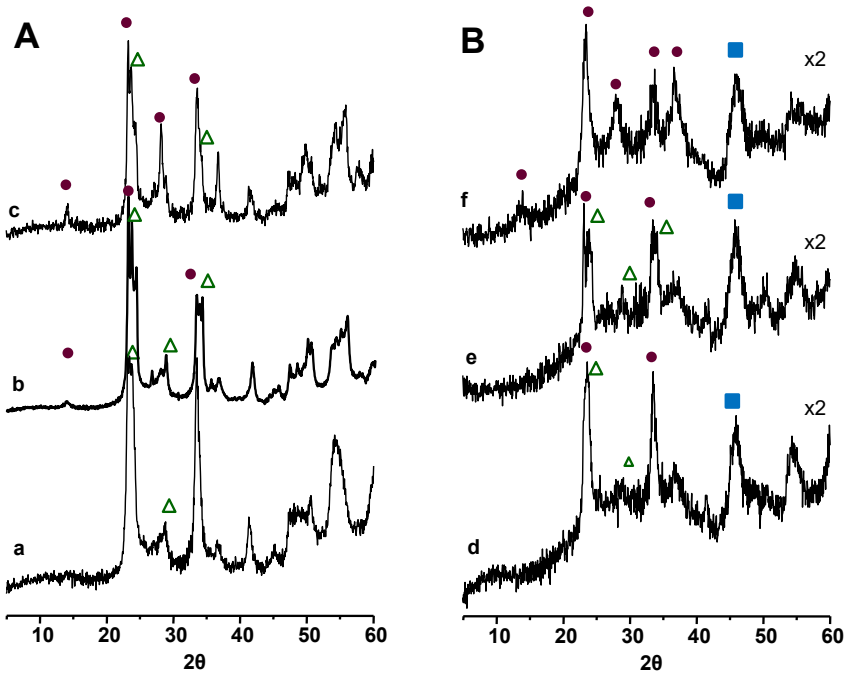

Fig. 1. XRD pattern of unsupported (A) and Al_2O_3-supported (B) W-V-O oxides: a) Sample **N-I**; b) Sample **N-II**; c) Sample **N-R**; d) Sample **S-I**; e) Sample **S-II**; f) Sample **S-R2**. Details reported in Table 1 and Table 2. Symbols: HTB structure (●); monoclinic WO_3 (Δ); γ-Al_2O_3 (■).

The characteristic reflections of tungsten oxide bronze with the HTB structure (at 2θ= 14.4, 23.0, 24.3, 27.2, 28.2º) (JCPDS no. 33-1387) are observed in samples **N-II** and **N-R** as well

as in sample **S-R2**. However, the unsupported samples (Fig. 1, pattern a) shows also the characteristics reflections of monoclinic WO_3 with peaks at 2θ= 23.1, 24.4 and 25.6º corresponding to (002), (020) and (200) reflections (JCPDS no. 43-1035).[38] According with the XRD results, γ-Al_2O_3 supported hexagonal bronze phase have been prepared following the procedure denoted as R. To study the influence of the vanadium content on the formation of the hexagonal phase supported on γ-Al_2O_3, the V/W atomic ratios in the synthesis gel (Fig. S2) has been varied (V/W atomic ratio of 1, 2 3) and the samples characterized by a series of techniques. A hexagonal phase (peaks at 2Θ = 14.4, 23.0, 24.3, 27.2, 28.2, 33.9, 36.9, 43.1, 44.9, 49.7, 55.9 and 58.27°) (JCPDS: 33-1387) (Fig. S2), more evident at intermediate V/W ratio (i.e. sample **S-R2**; Fig. 1B-pattern f and Fig. S2-pattern b), is present in all cases.[14] However, the phase purity of these materials is never complete, i.e. monoclinic phases are also likely present in the oxides (peaks at 2Θ = 23.1, 24.4, 25.6, and 34.2). On the other hand, Figure S3 (supplementary information) shows the XRD patterns of references materials, i.e. Al_2O_3-supported vanadium oxide (VOx/AL), W-V-O mixed oxides prepared hydrothermally (WV-HT), and Al_2O_3-supported W-V-O mixed oxides (V/W/AL) samples. The diffractograms are different to those of Fig. 1, as they do not show the peaks typical of the HTB phase.

To shed light on the distribution of the various phases in bulk and supported W-V-oxides, Raman spectroscopy was used as a characterization tool (Fig. 2A). Raman spectra of h-WO_3 and m-WO_3 reference samples show peaks at 783, 692, 648, 456, 325, 300, 264, and 185 cm^{-1},[41] and at 805, 714, 327, 289 cm^{-1},[41-43] respectively (Fig. S4). For V-containing WO_3, the Raman spectra of monoclinic and hexagonal h-$(WV)O_3$ phases prepared by hydrothermal synthesis give similar bands,[14] although some of them are shifted due to the different arrangement of the atoms in the two crystalline frameworks.[14,41] Particularly

indicative of the presence of one phase or the other is the O-W-O stretching vibrations which appears at higher wavenumbers (ca. 710 cm^{-1}) in the monoclinic (m-WO_3) phase than in the hexagonal (h-WO_3) one (ca. 693 cm^{-1}), which is probably due to the presence of reduced W-species ($W^{5+/6+}$) characteristic of the hexagonal phase.

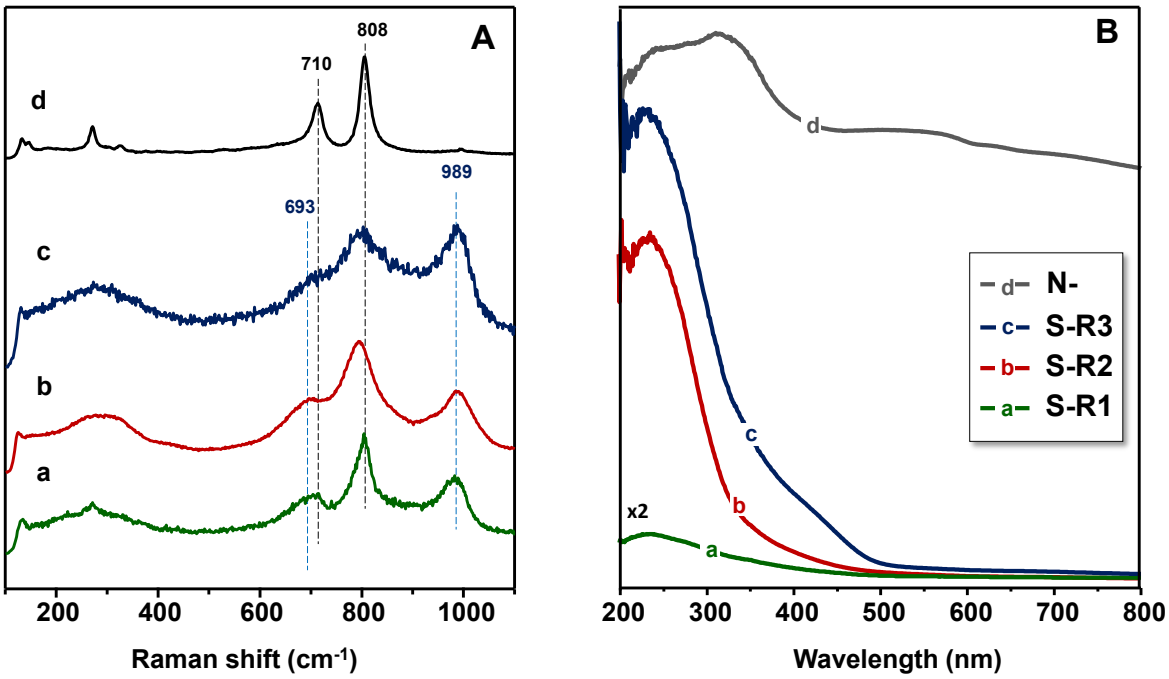

Fig. 2. Raman (A) and UV-Vis (B) spectra of unsupported (sample) and Al_2O_3-supported (a-c) and unsupported (d) W-V oxide bronzes. Catalysts: a) **S-R1**; b) **S-R2**; c) **S-R3**; d) **N-R**.

Raman spectra of Al_2O_3-supported W-V-O with different vanadium contents (Fig. 2A, spectra a to c) show bands in the 600-800 cm^{-1} region of W-O pairs and a band at 989 cm^{-1} related to the incorporation of V-species into the solids, that is, polymeric W-O-V-O-W entities with isolated octahedral VO_6 species.[44] Inspection of Figure 2A shows that phase purity (either completely monoclinic or hexagonal) is never obtained, although the higher

intensity of the band at 693 cm^{-1} in the alumina-supported W-V-O samples suggests a greater content of the hexagonal phase.[41] The broadness of the band at ca. 989 cm^{-1} in sample **N-R** (Fig. 2A, spectrum d) may indicate that besides isolated octahedral VO_6 species, polymeric V-species could be also present as minority.

UV-Vis spectroscopy can be used to study the local environment and oxidation state of transition metals. The presence of intense bands in the 200–500 nm region, attributed to ligand-to-metal charge transfer (LMCT), are related to presence of V^{5+} (d0) in the sample. The DR-UV-vis spectra of supported and unsupported W-V-O bronze catalysts with different V/W ratios are shown in Figure 2B (and those of reference catalysts in Figure S5). The presence of intense bands in the 200-300 nm region indicating the presence of V^{5+} is a common feature of all spectra.[45] In addition to this, the spectra of unsupported W-V-O samples, prepared by reflux (i.e. sample **N-R**; Fig. 2B, spectrum d), display also two bands in the 550-800 cm^{-1} region, which are due to V^{4+} in pseudo-octahedral coordination.[46]

In this way, it can be noticed that both V^{5+} (bands in the 240-350 nm range) and V^{4+} (bands in the 550-750 nm range) are observed in unsupported W-V-O bronze prepared hydrothermally (sample **WV-HT**) (Fig. S5, spectrum a), whereas mainly V^{5+} is observed in supported vanadium oxide, i.e. samples **VOx/AL**, **V/W/AL** and **VW/AL** (Fig. S5, spectra b to d, respectively). In addition, isolated tetrahedral VOx species (band at 250 nm) is mainly present in Al_2O_3-supported vanadium oxide (sample **VOx/AL**) (Fig. S5, spectra b), whereas polymeric VOx species (band at 350 nm) are observed in both vanadium oxide supported on WO_3/Al_2O_3 (sample **V/W/AL**) and in Al_2O_3-supported W-V-O (**VW/AL**) (Fig. S5, spectra c and d).

The amount of vanadyl VO^{2+} and/or V^{4+} species can be also of interest for explaining the catalytic performance (*vide infra*). This information can be gained from EPR experiments

(Fig. 3). The signals are characterized by key parameters, the g-factor and the hyperfine coupling constants (A), which in this case are related to the nature of vanadyl sites, giving information on the coordination geometry of the paramagnetic V^{4+} (d1) species. EPR is also a quantitative technique and allows the performance of experiments under *in situ* conditions.[47-51] Different EPR signals can be observed for vanadyl VO^{2+} species depending if they are isolated or polymeric.[47,48] Thus, isolated vanadyl VO^{2+} sites, formed e.g. in supported highly dispersed vanadia catalysts (low V-loading) give characteristic axial hyperfine structure so that the $g_{\perp}$, $g_{\parallel}$, $A_{\perp}$ and $A_{\parallel}$ can easily be extracted. Those splitting are averaged out in $(VO)_2P_2O_7$ in which the VO^{2+} sites are connected via oxygen bridges to form ladder-like double chains, and broad isotropic signals due to clustered V-O-V species are usually obtained in supported vanadium catalysts with medium V-loading.[50] Figure 3 shows the EPR spectra of representative V-containing tungsten bronze catalysts supported (i.e. **S-R1, S-R2** and **S-R3**) and unsupported (**N-R** sample), whereas the spectra of references (i.e., WV-HT, VOx/AL, V/W/AL, and WV/AL) are shown in Figure S6. Table 2 summarizes the characteristics of the EPR signals observed for every catalyst, as well as their axial distortion ($\Delta g_{\parallel}/\Delta g_{\perp}$), the in-plane delocation coefficient (β_2^{2*}) and the concentration of V^{4+} species.

Some of these spectra have been simulated to derive the spectral parameters and also to calculate the relative intensity of each signal, as illustrated in Figure 3B and 3C for samples **S-R2** and **N-R**, respectively (and in Fig. S7 for reference WV-HT sample). In general, the spectra can be simulated by considering two or three main components.

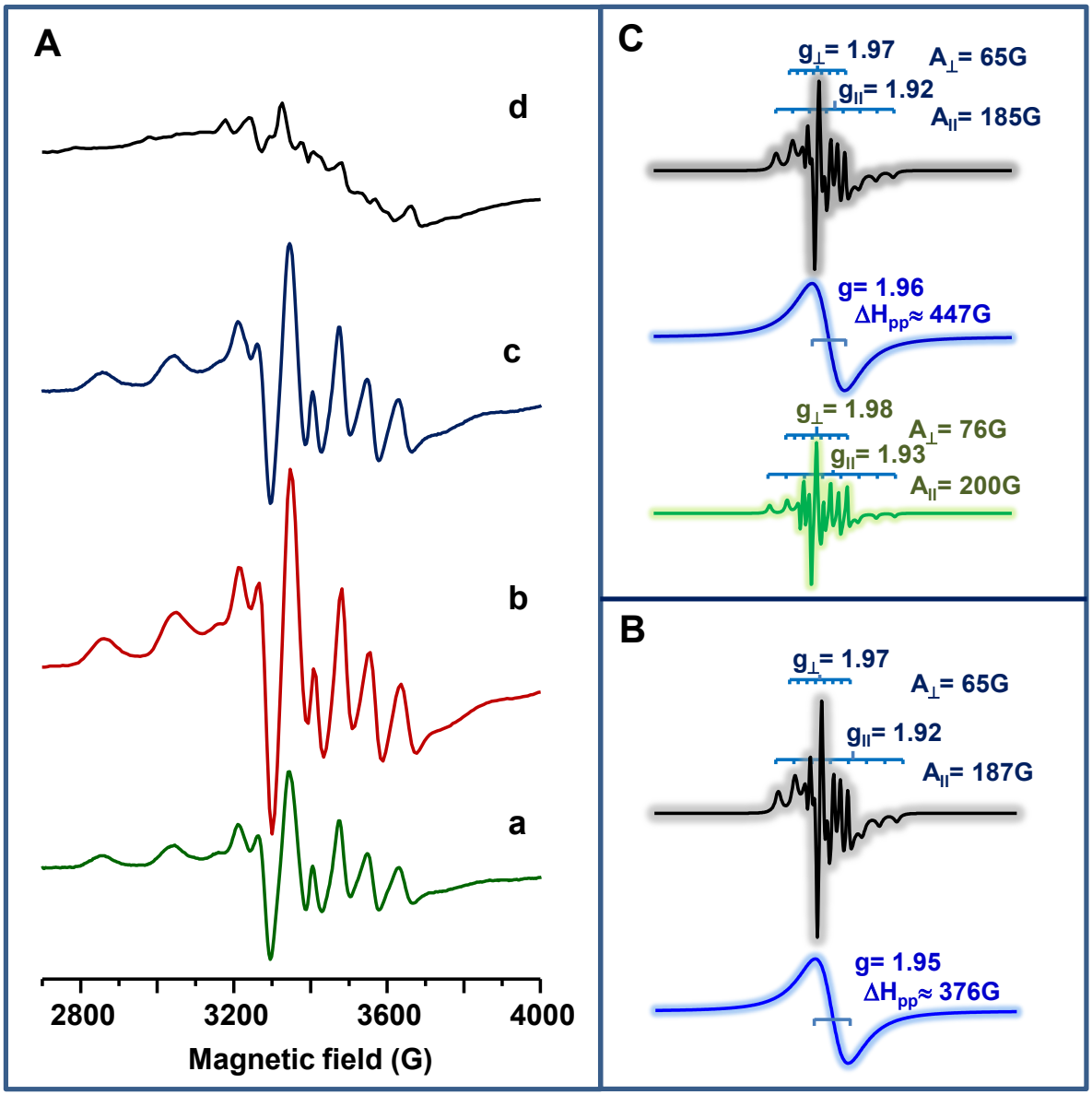

Fig. 3. EPR spectra of Al_2O_3-supported and unsupported W-V-O oxide bronzes (A): a) **S-R1**; b) **S-R2**; c) **S-R3**; d) **N-R**. Examples of simulation of the EPR spectra of sample **S-R2** (B) and **N-R** (C) with the corresponding deconvoluted spectra. The characteristics of each deconvoluted spectrum is also included.

The spectra of supported W-V-O bronzes (see Figure 3A, spectrum b) contains two signals (Fig. 3B): i) one isotropic broad component assigned to VO_x clusters dominant in sample **VOx/AL**;[51] and ii) one axially symmetric signal A with characteristic eight-line hyperfine

pattern due to the interaction of the unpaired electron with a ^{51}V nucleus (I=7/2) typical of an isolated VO^{2+} species (A-site).[47,48,50]

For unsupported W-V-O bronzes prepared by reflux (sample **N-R2**) (see Figure 3C) or hydrothermally (sample WV-HT, Fig. S7), the simulation of the EPR spectra shows the presence of two (instead of one) hyperfine structured signals with axial distortion (A- and B-sites) whose relative intensity depends on the catalyst.[47,48,50] The results obtained here suggest that the amount of isolated VO^{2+} sites is higher in supported V-containing tungsten bronze catalysts, especially sample **S-R2**, whereas the clustered vanadyl sites are more abundant in sample VOx/AL.

Finally, XPS results obtained for **N-R**, **S-R2** and reference catalysts are summarized in Table 3. The BE of the V 2p3/2 peaks are in the ranges 516.2-516.5 eV and 517.2-517.6 eV for V^{4+} and V^{5+} species, respectively.[52] The V^{4+}/V^{5+}ratio depends on the catalyst, being the highest for catalyst **S-R2** and the lowest for VOx/AL sample.[52-54] We must indicate that sample VOx/AL shows not only a peak at 517.2-517.6 eV (V^{5+} species) but also a peak at ca. 518.2 eV characteristic of highly dispersed V^{5+} species in supported vanadium oxide catalysts, as proposed previously.[55] This is in agreement to DR-UV-vis spectra (Fig. 2B and Fig. S5) but also with EPR results (Fig. 3).

The W 4f band can be decomposed into four peaks (two doublets) as presented in Fig. S8. The first doublet appears at binding energies of 35.2 and 37.4 eV for W^{6+} (W $4f_{7/2}$ and W $4f_{5/2}$, respectively), and the second doublet at 33.9 and 35.7 eV for W^{5+}.[56] The highest W^{5+}/W^{6+} ratio is observed for samples **S-R2** and WV-HT and the lower W^{5+}/W^{6+} ratio for **N-R** and V/W/AL. Since high W^{5+}/W^{6+} ratio is characteristic of tungsten oxide bronze,[14] it can be concluded that samples **S-R2** and WV-HT contain the highest concentration of W-

based bronze. This is in good agreement with the XRD (Fig. 1 and Fig. S2) and Raman (Fig. 2A and Fig. S4) results.

Figure 4 presents FE-SEM (Fig. 4A) and TEM (Fig. 4B) images, respectively of unsupported and supported W-V-O oxides catalysts prepared by reflux, i.e. samples **N-R** and **S-R2.** The unsupported sample (**N-R**) shows always platelet-shaped particles aggregates, whereas the corresponding supported sample (**S-R2**) shows smaller particle size.

A)

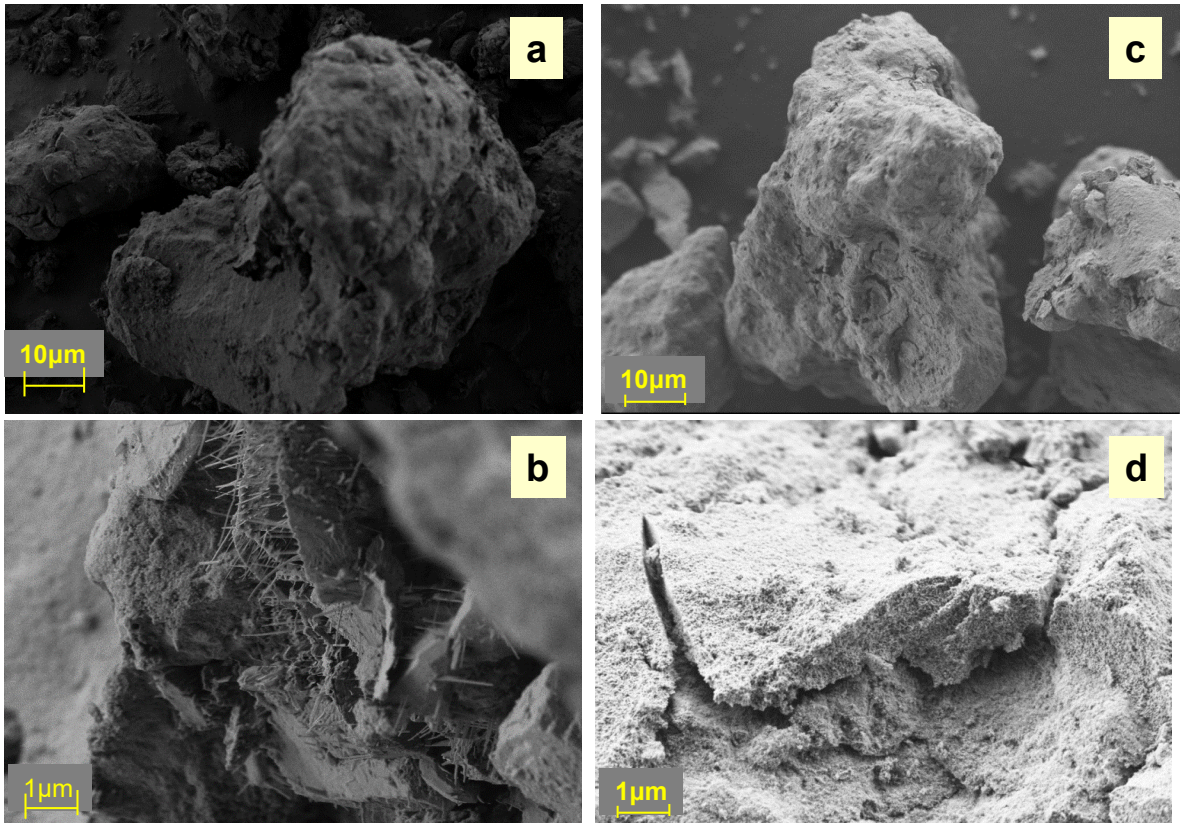

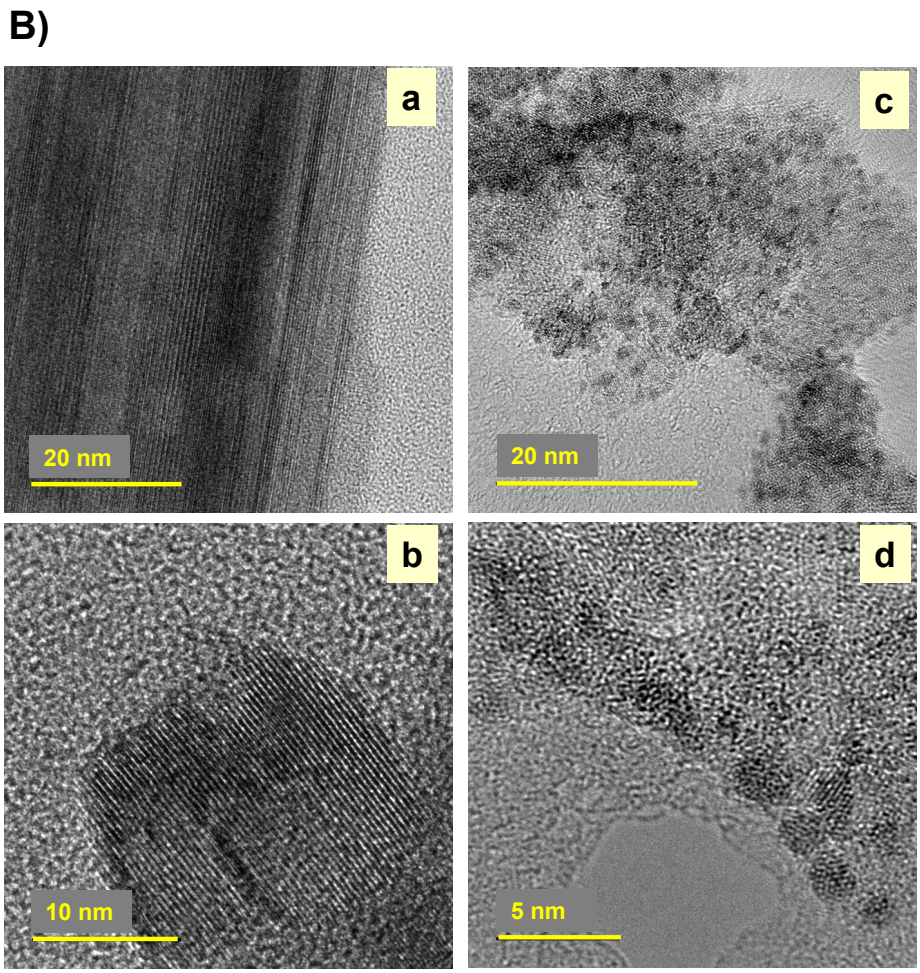

Fig. 4. FE-SEM (A) and TEM (B) of unsupported W-V-O (sample **N-R**) and Al_2O_3-supported W-V-O oxides (sample **S-R2**). Catalysts: **N-R** (a, b); **S-R2** (c, d).

Accordingly, 2D- and 3D-structures can be achieved depending on both the catalyst preparation procedure and catalyst composition. In this way, Figure 5 shows the main V-species observed in our catalysts: i) isolated vanadium species (A-sites) on the surface of small crystallites in alumina-supported W-V-O oxide bronzes; ii) isolated vanadium species in the bulk of relatively higher crystallites, in unsupported W-V-O bronzes, prepared by reflux or by hydrothermal synthesis; iii) polymeric VyOx clusters, in supported vanadium oxide catalysts.

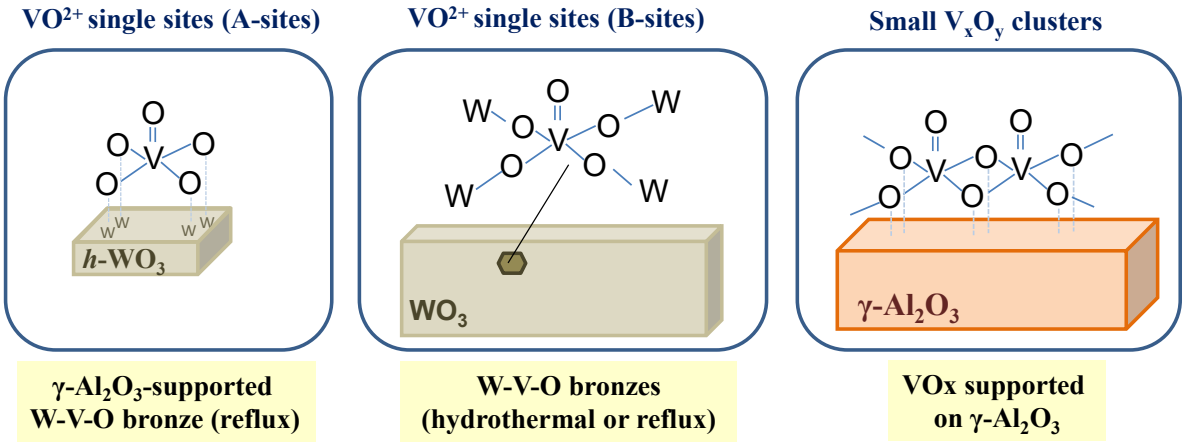

Fig. 5. Possible structures for the species experimentally observed in V-containing catalysts: A- and B-sites and small VxOy clusters.

Oxidative dehydrogenation of ethane

Among the W-V-O oxides prepared, representative samples were used as catalysts for the oxidative dehydrogenation of ethane, a reaction that has received considerable attention in the last years as a viable route for the on-purpose production of ethylene from natural gas.

When pure V-free hexagonal tungsten oxide bronze, *h*-WO_x (either supported or as bulk phase), was used as catalyst, no ethane conversion was registered in the reaction conditions used here, i.e. reaction temperatures lower than 450ºC. However, when vanadium was added to the structure, ethane was converted to reaction products. The catalytic behavior of supported W-V-O oxides bronzes with different V-content, i.e. samples **S-R1**, **S-R2** and **S-R3,** was studied as a function of the reaction temperature under standard conditions for ethane ODH (Figure 6).[22,39,40] It is clear that, for similar temperatures, ethane conversion is higher when the V-content of catalyst increases. Overall, the selectivity to ethylene decreases when increasing ethane conversion, mainly in favor of CO (Fig. 6c). At low

ethane conversion, no remarkable differences are observed between the three catalysts, but as the conversion increases sample **S-R2** shows a slightly higher selectivity to ethylene. This points out that an optimum V-content exists to increase the selectivity to ethylene, which is around V/W ratio of ca. 0.2.

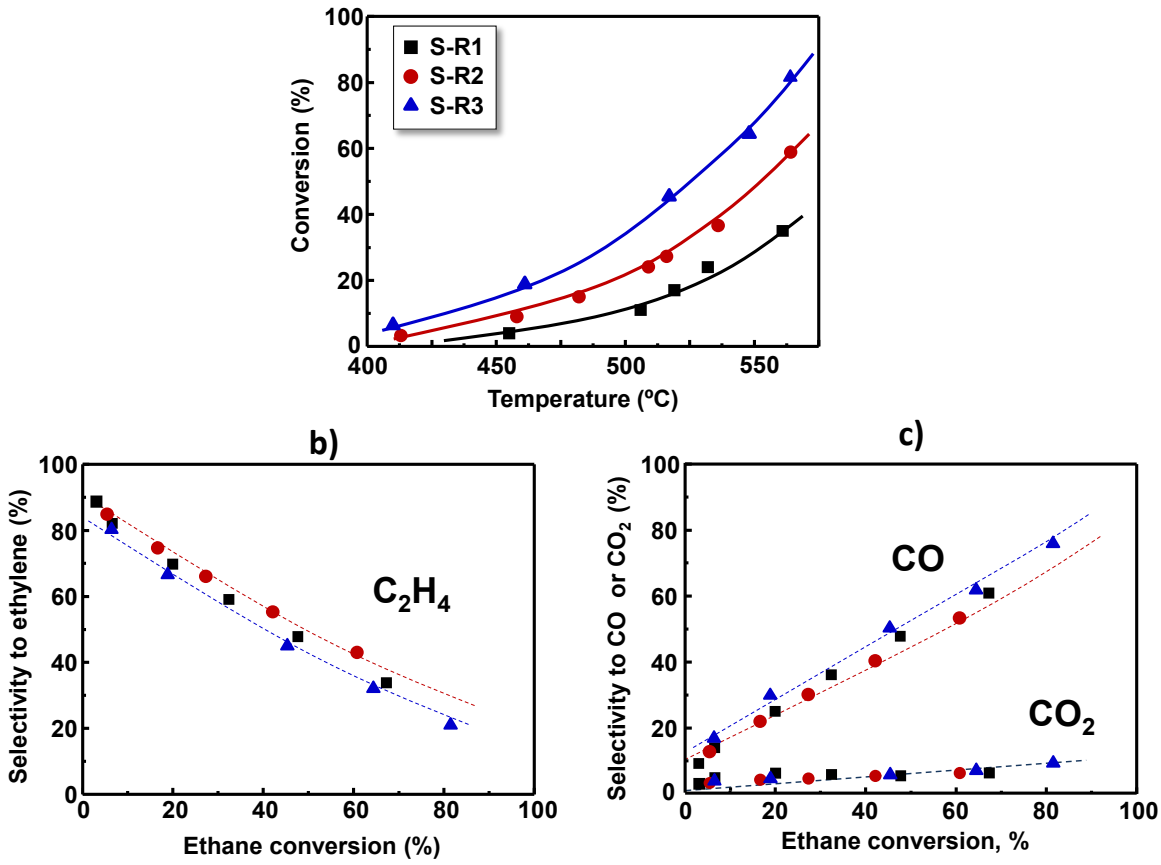

Fig. 6. Variation of ethane conversion vs. temperature (**a**) and variation of the selectivity to ethylene (**b**), and selectivity to CO and CO_2 (**c**) with ethane conversion during the Ethane ODH over Al_2O_3-supported W-V-O oxide bronzes: a) **S-R1**; b) **S-R2**; c) **S-R3**.

The general trends observed highlight that ethylene selectivity decreases when increasing the ethane conversion, whereas the selectivity to CO presents an opposite trend. Moreover,

the selectivity to CO_2 is in all cases very low and almost independent to conversion of ethane. Accordingly, it can be proposed the following reaction network, where $k_1 >> k_2$ and k_3 (Scheme 1).

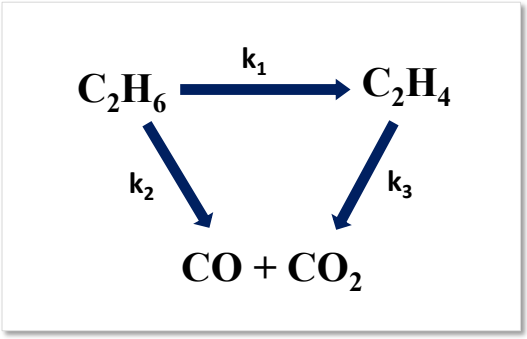

Scheme 1. Reaction network for the oxidative dehydrogenation of ethane over V-containing catalysts.

On the other hand, Figure 7 shows a comparison of the catalytic performance of sample **S-R2**, with those achieved over references: unsupported W-V-O bronze prepared by reflux (sample **N-R**) or hydrothermally (sample WV-HT), as well as for a vanadium supported over WO_x/Al_2O_3 (i.e. sample V/W/AL) or over an alumina-supported vanadium oxide catalysts, with a V-loading of 2 wt% of V-atoms (sample VO_x/AL**)**.

The latter are benchmark catalysts for ethane ODH.[20-24] All the materials reported in Figure 7 have a V-content ranging from 0.7 to 3.6 wt% (see Table S1). Both unsupported W-V-O samples (i.e. samples **N-R** and WV-HT) present a steep decrease in the ethylene selectivity as the conversion increases. Differently, when vanadium is supported on Al_2O_3, either as VO_x 2-D species in samples VOx/AL or as a hexagonal W-V-O-layer in sample V/W/AL, the pace at which the ethylene selectivity decreases as a function of conversion is drastically lower.

For sample VOx/AL the selectivity is known to increase as a function of V-loading, as long as 3D-Vanadium species are not formed (up to ca. 5 wt%).[17-23, 32-34,57]

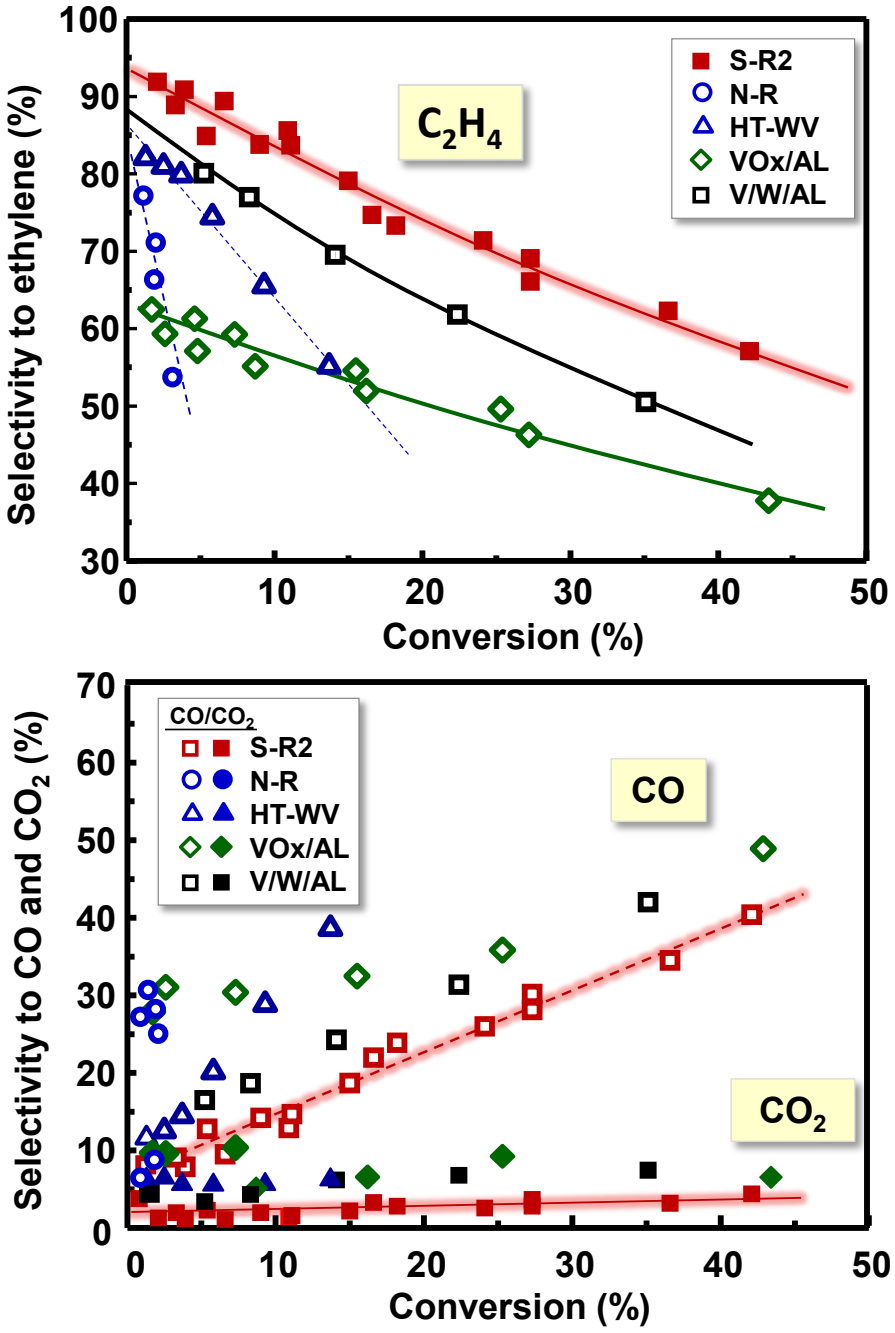

Fig. 7. Variation of the selectivity to ethylene (a) and CO and CO_2 (b) during the ethane ODH on V-containing catalysts in the 450-500ºC temperature range. Characteristics of catalysts in Table 1 and Table S1. Reaction conditions: Ethane/oxygen/nitrogen molar ratio of 4/8/88 and a contact time, W/F, of 80-240 g_{cat} h $(mol_{C2})^{-1}$.

The maximum yield obtained over alumina-supported vanadium oxide catalyst (VOx/AL) is about 16% (40% selectivity to ethylene at an ethane conversion of 40%). It must be stressed here the excellent performance of catalyst **S-R2** compared to the best Al_2O_3-supported vanadium oxide reported in the bibliography.[22,23]

Interestingly, even with a relatively low V-content (1.2 wt% V), sample **S-R2** outperforms the benchmark catalyst VOx/Al_2O_3: ethylene selectivity as high as 80% were recorded for ethane conversion around 18%. These values position the supported *h*-(WV)Ox catalyst (i.e. sample **S-R2**) as one of the most active and selective catalysts so far reported in the bibliography for ethane ODH over supported vanadium oxide catalysts,[17-19,21-24] outperformed only by the M1-phase catalysts [25-27] or some promoted NiO catalysts.[28-31]

According to these catalytic results and considering the characterization results, the behavior of these catalysts strongly depend on the nature of the V-sites. In fact when comparing DR-UV-vis, it can be seen how most catalysts show both tetrahedral and octahedral vanadium species, except sample **S-R2** in which octahedral coordination VO_6 species are predominant (Fig. 4). On the other hand, both DR-UV-vis (Fig. 2B) and EPR (Figs. 3) results confirm that the best supported V-W-O catalyst (sample **S-R2**) presents the higher amount of V^{4+}, and it appears that the EPR vanadyl species of type A are associated to a higher ethylene selectivity (see Table 2). Accordingly, the preparation procedure and/or the heat-treatment (or composition) favor changes in the characteristics of vanadium species.

In addition, it is possible that the relatively thin layer of V-containing hexagonal tungsten bronzes decreases over-oxidation since it hampers a "too fast" flow of bulk oxygen species.

Finally, a catalytic tests for approximately 70 hours shows that the **S-R2** catalyst is stable over time; the catalytic results show that for a conversion of ethane of 12% the selectivity to ethylene is around 80%, without changes during the time in which said study was carried out (Fig. S9).

Conclusions

V-containing hexagonal tungsten bronze supported on alumina has been successfully prepared by using a soft synthetic procedure (in a reflux for 16 h) and an adequate heat-treatment procedure (under N_2 at 600ºC using a rate of 100ºC min^{-1}). In this way, the structural characterization of heat-treated samples suggests that both unsupported and supported materials present hexagonal tungsten bronze (HTB) structure, although the crystal size of the HTB materials was smaller when supported on Al_2O_3. On the other hand, Raman, Diffuse Reflectance UV-vis and EPR results suggest partial substitution of V in the HTB structure, although different V-species are present depending on the V-loading and the catalyst composition. Thus, mainly isolated V-species are observed, but the proportion of tetrahedral and octahedral vanadium species strongly depend on the characteristics of catalysts. The Al_2O_3-supported V-W-O mixed oxides catalysts, with HTB structure, present an activity and selectivity to ethylene during the oxidative dehydrogenation of ethane higher than that observed for conventional supported vanadium oxide catalysts or unsupported V-containing HTB materials. In this way, it is known that the coordination of V atoms have different catalytic performance in C_2-C_4 ODH processes,[17-23,32-34,57] in which isolated tetrahedral V- species are relatively selective. However, in the case of ethane ODH, the less reactive alkane, and when working at relatively low temperature, more active V

sites are required in order to favor a rapid selective oxidative activation of ethane. In this, and according to our results, isolated octahedra V-species in an acid environment (as it is in hexagonal tungsten bronze),[14,38] mainly observed on the **S-R2** catalyst, seems to be the more selective sites in the oxidative dehydrogenation of ethane, reducing the importance of the rate of ethene combustion.

Conflict of interest

There are no conflicts to declare

Acknowledgments

The authors acknowledge the DGICYT in Spain (Projects RTI2018-099668-B-C21, and SEV-2016-0683) for financial support. The research group of Prof. Fabrizio Cavani (University of Bologna, Italy) and Consorzio INSTM (Firenze) are gratefully acknowledged for a PhD grant to A.C. Authors also thank the Electron Microscopy Service of Universitat Politecnica de Valencia for their support.

Notes and References

1. a) J.-D. Guo and M.S. Wittingham, *Int. J. Mod. Phys. B,* 1993, **7**, 4145- 4164; b) M.S. Wittingham, J.-D. Guo, R. Chen, T. Churayil, G. Janauer and P. Zabalij, S*olid State Ionics,* 1995, **75**, 257-268.
2. J. Chen, H. Wang, J. Deng, C. Xu and Y. Wang, *J. Mat. Chem. A*, 2018, **6**, 8986-8991.
3. a) L. Bartha, A.B. Kiss and T. Szalay, *Int. J. Refract. Met. Hard. Mater.,* 1995, **13**, 77-91; b) R.J.D. Tilley, *Int. J. Refract. Met. Hard. Mater.,* 1995, **13**, 93-109.
4. A. Michailovski, F. Krumeich, and G.R. Patzke, *Chem. Mater.,* 2004, **16**, 1433-1440;
5. H. Quan, Y. Gao and W. Wang, *Inorg. Chem. Front.,* 2020, **7**, 817–838.

6. a) A. Michailovski and G.R. Patzke, *Chem. Eur. J.*, 2006, **12**, 9122 –9134; b) A. Michailovski, R. Kiebach, W. Bensch, J.-D. Grunwaldt, A. Baiker, S. Komarneni and G.R. Patzke, *Chem. Mater.*, 2007, **19**, 185-197.
7. R. Kiebach, N. Pienack, W. Bensch, J.-D. Grunwaldt, A. Michailovski, A. Baiker, T. Fox, Y. Zhou and G.R. Patzke, *Chem. Mater.*, 2008, **20**, 3022–3033.
8. A. Magneli and B. Blomberg, *Acta Chem. Scand.,* 1951, 5, 372-378.
9. C.N.R. Rao and K. Biswas, Soft Chemistry Routes, in *Essentials of Inorganic Materials Synthesis*, Eds: C.N.R. Rao, K. Biswas, John Wiley & Sons, Inc., New Jersey, 2015, Ch. 10.
10. F. Li, Y. Qian and A. Stein, *Chem. Mater.*, 2010, **22**, 3226–3235.
11. J. Gopalakrishnan, *Chem. Mater*., 1995, **7**, 1265–1275
12. S. Stevenson and P.A. Sermon, *J. Chem. Soc., Faraday Trans. I*, 1987, **83**, 2175-2191.
13. I.M. Szilágyi, F. Hange, J. Madarász and G, Pokol, *Eur. J. Inorg. Chem.* 2006, 3413–3418.
14 M. D. Soriano, P. Concepcion, J. M. López Nieto, F. Cavani, S. Guidetti and C. Trevisanut, *Green Chem.,* 2011, **13**, 2954-2962
15. E. Garcia-González, M. D. Soriano, E. Urones-Garrote and J. M. López Nieto, *Dalton Trans.*, 2014, **43**, 14644-14652.
16. A. Chieregato, J.M. López Nieto, F. Cavani, *Coord. Chem. Rev.,* 2015, **301-302**, 3-23.
17. F. Cavani, N. Ballarini and A. Cericola, *Catal. Today*, 2007, **127**, 113-131.
18. C.A. Gartner, A.C. van Veen and J.A. Lercher, *ChemCatChem*, 2013, **5**, 3196-3217.
19. P. Kube, B. Frank, S. Wrabetz, J. Kröhnert, M. Hävecker, J. Velasco-Vélez, J. Noack, R. Schlögl and A. Trunschke, *ChemCatChem*, 2017, **9**, 573-585.
20. X. Rozanska, R. Fortrie and J. Sauer, *J. Am. Chem. Soc.,* 2014, **136**, 7751-7761.
21. A. Dinse, R. Schomäcker and A.T. Bell, *Phys. Chem. Chem. Phys.*, 2009, **11**, 6119–6124
22. T. Blasco, A. Galli, J.M. López Nieto and F. Trifiró, *J. Catal.*, 1997, **169**, 203-211.
23. M.D. Argyle, K. Chen, A.T. Bell and E. Iglesia, *J Catal.*, 2002, **208**, 139–149.

24. Al-Ghamdi, M. Volpe, M.M. Hossain and H. de Lasa, *Appl. Catal. A: Gen.*, 2013, **450**, 120-130.
25. B. Solsona, M.I. Vázquez, F. Ivars, P. Concepción and J.M. López Nieto, *J. Catal.*, 2007, **252**, 271-280
26. J.M. López Nieto, P. Botella, M.I. Vázquez and A. Dejoz, US 7,319,179 B2 (2008); *assigned to UPV-CSIC*.
27. A.M. Gaffney and O.M. Mason, *Catal. Today*, 2017, **285**, 159-165.
28. E. Heracleous and A.A. Lemonidou, *J. Catal.*, 2006, **237**, 162−174.
29. D. Ipsakis, E. Heracleous, L. Silvester, D.B. Bukur and A.A. Lemonidou, *Chem. Eng. J.,* 2017, **308**, 840−852
30. B. Solsona, P. Concepcion, J.M. López Nieto, A. Dejoz, J.A. Cecilia, S. Agouram, M.D. Soriano, V. Torres, J. Jiménez-Jiménez and E. Rodríguez Castellón, *Catal. Sci. Technol.,* 2016, **6**, 3419−3429.
31. H. Zhu, D.C. Rosenfeld, M. Harb, D.H. Anjum, M.N. Hedhili, S. Ould-Chikh, and J.-M. Basset, *ACS Catal.*, 2016, **6**, 2852-2866.
32. C.A. Carrero, S.P. Burt, F. Huang, J.M. Venegas, A.M. Love, Ph. Mueller, H. Zhu, J.T. Grant, R. Mathison, M.P. Hanraham, A. Rossini, M. Ball, J. Dumesic and I. Hermans, *Catal. Sci. Technol.,* 2017, **7**, 3707-3714.
33. A.M. Love, C. A. Carrero, A. Chieregato, J.T. Grant, S. Conrad, R. Verel and I. Hermans, *Chem. Mater.*, 2016, **28**, 5495-5504.
34. J.T. Grant, C.A. Carrero, A.M. Love, R. Verel and I. Hermans, *ACS Catal.,* 2015, **5**, 5787-5793.
35. S. Barman, N. Maity, K. Bhatte, S. Ould-Chikh, O. Dachwald, C. Haeßner, Y. Saih, E. Abou-Hamad, I. Llorens, J.-L. Hazemann, K. Köhler, V. D' Elia and J.-M. Basset, *ACS Catal.*, 2016, 6, 5908-5921.
36. G. J. Maffia, A.M. Gaffney and O.M. Mason, *Top. Catal.*, 2016, **59**, 1573-1579.
37. M. Sanati and A. Andersson, *J. Mol. Catal.,* 1990, **59**, 233–255.
38. M. D. Soriano, A. Chieregato, S. Zamora, F. Basile, F. Cavani and J.M. López Nieto, *Top. Catal.*, 2016, **59**, 178-185.
39. B. Solsona, A. Dejoz, T. Garcia, P. Concepcion, J.M. López Nieto, M.I. Vázquez and M.T. Navarro, *Catal. Today*, 2006, **117**, 228-233.

40. P. Botella, A. Dejoz, M.C. Abello, M.I. Vázquez, L. Arrua and J.M. López Nieto, *Catal. Today*, 2009, **142**, 272-277.
41. Sh.F. Shaikh, Sh.S. Kalanur, R.S. Mane and O.-Sh. Joo, *Dalton Trans.*, 2013, **42**, 10085-10088.
42. I. M. Szilagyi, J. Madarasz, G. Pokol, P. Kiraly, G. Tarkanyi, S. Saukko, J. Mizsei, A.L. Toth, A. Szabo and K. Varga-Josepovits, *Chem. Mater.,* 2008, **20**, 4116-4125.
43. S.S. Chan, I.E. Wachs, L.L. Murrell and N.C. Dispenziere, *J. Catal.*, 1985, **92**, 1-10.
44. G. Deo, F. D. Hardcastle, M. Richards, A. M. Hirt and I.E. Wachs, In Novel Materials in Heterogeneous Catalysis; Baker, R., et al. (Editors); ACS Symposium Series; American Chemical Society: Washington, DC, 1990, pp. 317.
45. M.C. Kaezer França, R. A. da Silva San Gil and J.-G. Eon, *Catal. Today*, 2003, **78**, 105–115.
46. G. Catana, R. R. Rao, B. M. Weckhuysen, P. Van Der Voort, E. Vansant and R.A. Schoonheydt, *J. Phys. Chem. B*, 1998, 102, 8005-8012.
47. A. Bruckner, *Chem. Soc. Rev.*, 2010, 39, 4673-4684.
48. A. Brückner, *Top. Catal.,* 2006, **38**, 133-139.
49 Z. Strassberger, E.V. Ramos-Fernández, A. Boonstra, R. Jorna, S. Tanase and G. Rothenbergm, *Dalton Trans.*, 2013, **42**, 5546-5553.
50. P.G.W.A. Kompio, A. Brückner, F. Hipler, G., Auer, E. Löffler and W. Grünert, *J. Catal.*, 2012, **286**, 237-247.
51. P. Concepcion, H. Knözinger, J. M. López Nieto and A. Martinez-Arias, *J. Phys. Chem. B,* 2002, **106**, 2574-2582.
52. G. Silversmit, D. Depla, H. Poelman, G.B. Marin and R. De Gryse, *J. Electron Spectrosc.*, 2004, **135**, 167-175.
53. Y. Suchorski, L. Rihko-Struckmann, F. Klose, Y. Ye, M. Alandijska, K. Sundmacher and H. Weiss, *Appl. Surf. Sci.,* 2005, **249**, 231-237.
54. F. Klose, T. Wolff, H. Lorenz, A. Seidel-Morgenstern, Y. Suchorski, M. Piórkowska and H. Weiss, *J. Catal.*, 2007, **247**, 176–193.
55. C. Hess, G. Tzolova-Müller and R. Herbert, *J. Phys. Chem. C*, 2007, **11**, 9471-9479.
56. Y. Liu, S. Sherestha and W.E. Mustain, *ACS Catal.*, 2012, **2**, 456-463.
57. J.M. López Nieto, *Top. Catal.*, 2006, **43**, 3-15.

Table 1. Characteristics of catalysts.

Catalyst	Support	Preparation method (step) [a]			V/(W+ V) ratio		Surface area
		1	2	3	Theoretical	EDX [b]	(m^2 g^{-1})
N-I	None	OA	V-salt	Reflux	0.20	0.12	9.6
N-II	None	OA	Reflux	V-salt	0.20	0.16	n.d.
N-R	None	Reflux	OA	V-salt	0.20	0.20	1.1
S-I	γ-Al_2O_3	OA	V-salt	Reflux	0.20	0.17	122
S-II	γ-Al_2O_3	OA	Reflux	V-salt	0.20	0.20	n.d.
S-R1	γ-Al_2O_3	Reflux	OA	V-salt	0.10	0.07	118
S-R2	γ-Al_2O_3	Reflux	OA	V-salt	0.20	0.17	119
S-R3	γ-Al_2O_3	Reflux	OA	V-salt	0.30	0.29	127

a) Step in which oxalic acid (OA) and Vanadyl Sulphate (VS) are incorporated to an aqueous solution of APT, as well as step in which the reflux of components is carried out; b) V/(W + V) ratio obtained by XEDS.

Table 2. Simulated parameters of the EPR spectra of W-V-based catalysts and parameters calculated thereof, (axial distortion of VO^{2+} sites), and concentration of V^{4+} species. [1]

Sample	Site	$g_{\parallel}$	g	$g_{\perp}$	$A_{\parallel}$	ΔH_{pp}/G	$A_{\perp}$(G)	$\Delta g_{\parallel}/\Delta g_{\perp}$	β_2^{2*}	V^{4+} (%)	Site A (%)	Selectivity (%)[2]
N-R	A	1.922		1.972	185		65	2.64	0.70	0.09	0.002	
	B	1,929		1.978	200		76	2.96	0.74			
	Singlet		1.960			447						
S-R1	A	1.919		1.972	185		64	2.70	0.74	0.10	0.09	71
	Singlet		1.955			376						
S-R2	A	1.915		1.970	187		65	2.75	0.72	0.24	0.10	73
	Singlet		1.954			376						
S-R3	A	1.921		1,972	185		63	2.69	0.73	0.16	0.08	67
	Singlet		1,959			380						
WV-HT	A	1.922		1.972	185		65	2.65	0.71	0.04	0.001	40
	B	1.929		1.977	200		76	2.89	0.74			
	Singlet		1.960			490						
V/W/AL	A		n.d									
	Singlet		n.d									
VOx/AL	A		n.d							0.06		50

1) Axial distorsion of VO^{2+} sites ($\Delta g_{\parallel}/\Delta g_{\perp}$); in-plane delocation coefficient (β_2^{2*}).
2) Selectivity to ethylene at an ethane conversion of 25%.
3) ΔH_{pp} is the width measured from peak to peak

Table 3. XPS Results of representative W-V-based catalysts.

Sample	Surface atomic ratio	V2p3/2		W4f7/2		Al2p
	O/Al/W/V	V^{4+}	V^{5+}	W^{5+}	W^{6+}	Al^{3+}
N-R	68.12/0.0/28.80/3.08	516.2 (38.6%)	517.5 (61.4%)	35.1 (27.1%)	35.8 (72,9%)	-
S-R2	61.90/31.79/5.87/0.44	516.3 (58.4%)	517.5 (41.6%)	35.6 (53.8%)	36,4 (46.2%)	74.5
WV-HT	69.50/0.0/27.98/2.53	516.2 (38.7%)	517.2 (61.3)	35.4 (45.7%)	36.1 (54.3%)	-
VOx/AL	53.28/46.04/0.0/0.68	-	517.0 (55.0%) 518.2 (45.0%)	-	-	74.5
V/W/AL	54.69/40.42/3.97/0.91	516.5 (20.8%)	517.8 (79.2%)	35.6 (33.9%)	36.5 (66.1%)	74.4

Caption to figures

Fig. 1. XRD pattern of unsupported (A) and Al_2O_3-supported (B) W-V-O oxides: a) Sample **N-I**; b) Sample **N-II**; c) Sample **N-R**; d) Sample **S-I**; e) Sample **S-II**; f) Sample **S-R2**. Details reported in Table 1 and Table 2. Symbols: HTB structure (●); monoclinic WO_3 (Δ); γ-Al_2O_3 (■).

Fig. 2. Raman (A) and UV-Vis (B) spectra of unsupported (sample) and Al_2O_3-supported (a-c) and unsupported (d) W-V oxide bronzes. Catalysts: a) **S-R1**; b) **S-R2**; c) **S-R3**; d) **N-R**.

Fig. 3. EPR spectra of Al_2O_3-supported and unsupported W-V-O oxide bronzes (A): a) **S-R1**; b) **S-R2**; c) **S-R3**; d) **N-R**. Examples of simulation of the EPR spectra of sample **S-R2** (B) and **N-R** (C) with the corresponding deconvoluted spectra. The characteristics of each deconvoluted spectrum is also included.

Fig. 4. FE-SEM (A) and TEM (B) of unsupported W-V-O (sample **N-R**) and Al_2O_3-supported (sample **S-R2**) W-V-O oxides. Catalysts: **N-R** (a, b); **S-R2** (c, d).

Fig. 5. Possible Structures for the species experimentally observed in V-containing catalysts: A- and B-sites and small VxOy clusters.

Fig. 6. Variation of ethane conversion vs temperature (**a**) and variation of the selectivity to ethylene (**b**), and selectivity to CO and CO_2 (**c**) with ethane conversion during the ethane ODH over Al_2O_3-supported W-V oxide bronzes: a) **S-R1**; b) **S-R2**; c) **S-R3**.

Fig. 7. Variation of the selectivity to ethylene (a) and selectivity to CO and CO_2 (b) during the ethane ODH on V-containing catalysts. Characteristics of catalysts in Table 1 and Table S1. Reaction conditions: Ethane/oxygen/nitrogen molar ratio of 4/8/88 and a contact time, W/F, of 80-240 g_{cat} h $(mol_{C2})^{-1}$.

Scheme 1. Reaction network for the oxidative dehydrogenation of ethane over V-containing catalysts.

For Table of Contents Use Only